Aromaticity and Antiaromaticity in 4-, 6-, 8-, and 10-Membered Conjugated Hydrocarbon Rings†

Simon C. A. H. Pierrefixe and F. Matthias Bickelhaupt*

Department of Theoretical Chemistry and Amsterdam Center for Multiscale Modeling, Scheikundig Laboratorium der Vrije Universiteit, De Boelelaan 1083, NL-1081 HV Amsterdam, The Netherlands

Received: January 18, 2008; Revised Manuscript Received: March 4, 2008

Recently, we presented a molecular orbital (MO) model of aromaticity that explains, in terms of simple orbital-overlap arguments, why benzene (C_6H_6) has a regular structure with delocalized double bonds whereas the geometry of 1,3-cyclobutadiene (C_4H_4) is distorted with localized double bonds. Here, we show that the same model and the same type of orbital-overlap arguments also account for the irregular and regular structures of 1,3,5,7-cyclooctatetraene (C_8H_8) and 1,3,5,7,9-cyclodecapentaene ($C_{10}H_{10}$), respectively. Our MO model is based on accurate Kohn−Sham DFT analyses of the bonding in C_4H_4, C_6H_6, C_8H_8, and $C_{10}H_{10}$ and how the bonding mechanism is affected if these molecules undergo geometrical deformations between regular, delocalized ring structures and distorted ones with localized double bonds. The propensity of the π electrons is always to localize the double bonds, against the delocalizing force of the σ electrons. Importantly, we show that the π electrons nevertheless determine the localization (in C_4H_4 and C_8H_8) or delocalization (in C_6H_6 and $C_{10}H_{10}$) of the double bonds.

1. Introduction

Aromaticity and antiaromaticity of compounds have been the subject of many experimental and theoretical studies.[1,2] The key characteristics of aromatic compounds are the following: (i) a regular, delocalized structure involving C−C bonds of equal length, each with partial double-bond character, (ii) enhanced thermodynamic stability, and (iii) reduced reactivity as compared to nonaromatic conjugated hydrocarbons. Antiaromatic compounds show exactly the opposite. They have (i) an irregular structure with alternating single and localized double C−C bonds, (ii) reduced thermodynamic stability, and (iii) enhanced reactivity.

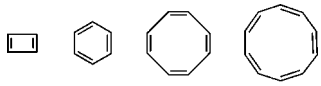

1 **2** **3** **4**

Recently, in a quantitative Kohn−Sham molecular orbital (MO) study, we addressed the question why the antiaromatic 1,3-cyclobutadiene (**1**) and aromatic benzene rings (**2**) have localized and delocalized structures, respectively.[3] Our MO model showed that the π-electron system never favors a symmetric, delocalized ring, neither in **1** nor in **2**. The regular, symmetric structure of benzene (**2**) appears to have the same cause as that of planar cyclohexane, namely, the σ-electron system. And yet, maybe somewhat counterintuitively at first sight, it is the π system which determines whether delocalization occurs. The mechanism behind this control is a qualitatively different geometry-dependence of the π overlap in **1** and **2**. In the aromatic species **2**, the localizing propensity of the π system emerges from a subtle interplay of counteracting overlap effects and is therefore too little pronounced to overcome the delocalizing σ system. On the contrary, in the antiaromatic ring **1**, all π overlap effects unidirectionally favor localization of the double bonds and can, in this way, overrule the σ system.[3]

Our work echoes earlier theoretical and experimental studies on aromaticity. Initially, Hückel ascribed the driving force for delocalization in benzene and other circularly conjugated $4n + 2$ π-electron species to the π-electron system.[4,5] Note that this disagrees in a subtle, yet essential manner, with our findings.[3] The latter points to a key role for the π electrons in determining whether localization of the double bonds occurs but they do so as a regulating factor, not as the driving force for this localization. In fact, evidence against the idea that benzene's D_{6h} symmetric structure originates from a delocalizing propensity of its π-electron system has been reported already since the late 1950s.[6,7] Shaik, Hiberty, and co-workers[8] showed in terms of an elegant valence bond (VB) model that it is the σ system that enforces the delocalized D_{6h} symmetric structure of **2** upon the π system, which intrinsically strives for localized double bonds. These conclusions initiated a debate[9] but were eventually reconfirmed by others;[3,10] this includes our MO model of aromaticity which nicely improves and confirms the modern VB picture developed by Shaik and Hiberty.

The purpose of the present paper is to explore whether our MO model developed for 1,3-cyclobutadiene (**1**) and benzene (**2**) also extends to the next larger, formally Hückel-antiaromatic ($4n$ π electrons) and Hückel-aromatic ($4n + 2$ π electrons) conjugated hydrocarbons rings: 1,3,5,7-cyclooctatetraene (**3′**) and 1,3,5,7,9-cyclodecapentaene (**4′**). Note that **3′** and **4′** are no longer planar species as would be suggested by the qualitative structures **3** and **4**, shown above.[5,11] Instead, cyclooctatetraene (**3′**) is a tub-shaped molecule with localized double bonds, as shown somewhat more realistically below.[11a] Also, cyclodecapentaene adopts only nonplanar conformations, such as the boat- or saddle-shaped C_2 symmetric species, shown in **4′** (twist conformation).[11b]

† Part of the "Sason S. Shaik Festschrift".

* E-mail: FM.Bickelhaupt@few.vu.nl.

10.1021/jp800514n CCC: $40.75
Published on Web 05/10/2008

Interestingly, cyclodecapentaene, as compared to benzene, shows an increased tendency to localize its double bonds, although it is formally aromatic according to Hückel's $4n + 2$ π-electron rule, with $n = 2$. Schaefer and co-workers[11b] have carried out an extensive exploration of the various conformations of **4**. They found that a C_2 symmetric conformation, as shown schematically in **4′**, is the lowest in energy at CCSD(T)//MP2. Furthermore, they found that whether the double bonds are delocalized or localized depends critically on the level of theory, but also on which particular conformation was considered. Conformation **4′** was found to localize its double bonds. On the other hand, the heart-shaped conformation **4″**, which is only 4.2 kcal/mol higher in energy than **4′**, was found to adopt a more delocalized structure with pronounced partial double-bond character in all C−C bonds.[11b] This behavior contrasts with the pronounced and robust propensity of benzene to adopt a symmetric, delocalized structure (**2**).[3,5]

Thus, we have quantum chemically investigated the structure and bonding of **1**, **2**, **3**, **3′**, **4**, and **4′** at the BP86/TZ2P level of density functional theory (DFT) by using the Amsterdam density functional (ADF) program.[12] Our analyses show that the MO model developed previously for **1** and **2** is indeed also valid for **3** and **4**. The π-electron system is confirmed to have in all cases a propensity to localize double bonds against the delocalizing force of the σ-electron system. This propensity is however only weakly pronounced in the case of the aromatic species (**2** and **4**). Simple orbital-overlap arguments account for this behavior as well as for the fact that the tendency of the π-electron system to localize the double bonds becomes stronger if one goes from the smaller benzene (**2**) to the larger cyclodecapentaene ring (**4**).

2. Theoretical Methods

2.1. General Procedure. All calculations were performed by using the ADF program developed by Baerends et al.[12] The numerical integration was performed by using the procedure developed by te Velde et al.[12g,h] The MOs were expanded in a large uncontracted set of Slater-type orbitals (STOs) containing diffuse functions, TZ2P (no Gaussian functions are involved).[12i] The basis set is of triple-ζ quality for all atoms and has been augmented with two sets of polarization functions, that is 3d and 4f on C and 2p and 3d on H. The 1s core shell of carbon was treated by the frozen-core approximation.[12c] An auxiliary set of s, p, d, f, and g STOs was used to fit the molecular density and to represent the Coulomb and exchange potentials accurately in each self-consistent field cycle.[12j]

Equilibrium structures were optimized by using analytical gradient techniques.[12k] Geometries and energies were calculated at the BP86 level of the generalized gradient approximation: exchange is described by Slater's Xα potential[12l] with corrections from Becke[12m,n] added self-consistently, and correlation is treated in the Vosko−Wilk−Nusair parameterization[12o] with nonlocal corrections from Perdew[12p] added, again, self-consistently (BP86).[12q] All stationary points were confirmed to be equilibrium structures (number of imaginary frequencies = NIMAG = 0), transition states (NIMAG = 1), or higher-order saddle points (NIMAG > 1) through vibrational analysis.

2.2. Bonding Energy Analysis. To obtain more insight into the nature of the bonding in our antiaromatic (**1** and **3**) and aromatic (**2** and **4**) systems, an energy-decomposition analysis has been carried out.[13] In this analysis, the total binding energy ΔE associated with the formation of the overall molecular species of interest, say AB, from two (or sometimes more) radical fragments, A′ + B′, is made up of two major components (eq 1):

$$\Delta E = \Delta E_{\text{prep}} + \Delta E_{\text{int}} \tag{1}$$

In this formula, the preparation energy ΔE_{prep} is the amount of energy required to deform the individual (isolated) radical fragments from their equilibrium structure (A′, B′) to the geometry that they acquire in the overall molecule (A, B). The interaction energy ΔE_{int} corresponds to the actual energy change when these geometrically deformed fragments A and B are combined to form the combined molecular species AB. It is analyzed in the framework of the Kohn−Sham MO model by using a quantitative decomposition of the bond into electrostatic interaction, Pauli repulsion (or exchange repulsion or overlap repulsion), and (attractive) orbital interactions (eq 2).[13]

$$\Delta E_{\text{int}} = \Delta V_{\text{elstat}} + \Delta E_{\text{Pauli}} + \Delta E_{\text{oi}} \tag{2}$$

The term ΔV_{elstat} corresponds to the classical electrostatic interaction between the unperturbed charge distributions $\rho_A(r) + \rho_B(r)$ of the prepared or deformed radical fragments A and B (vide infra for definition of the fragments) that adopt their positions in the overall molecule AB and is usually attractive. The Pauli repulsion term, ΔE_{Pauli}, comprises the destabilizing interactions between occupied orbitals and is responsible for the steric repulsion. This repulsion is caused by the fact that two electrons with the same spin cannot occupy the same region in space. It arises as the energy change associated with the transition from the superposition of the unperturbed electron densities $\rho_A(r) + \rho_B(r)$ of the geometrically deformed but isolated radical fragments A and B to the wavefunction $\Psi^0 = N\hat{A}\,[\Psi_A\,\Psi_B]$, that properly obeys the Pauli principle through explicit antisymmetrization ($\hat{A}$ operator) and renormalization (N constant) of the product of fragment wavefunctions (see ref 13a for an exhaustive discussion). The orbital interaction ΔE_{oi} in any MO model, and therefore also in Kohn−Sham theory, accounts for electron-pair bonding,[13a,b] charge transfer (i.e., donor−acceptor interactions between occupied orbitals of one moiety with unoccupied orbitals of the other, including the HOMO−LUMO interactions), and polarization (empty−occupied orbital mixing on one fragment due to the presence of another fragment). In the bond-energy decomposition, open-shell fragments are treated with the spin-unrestricted formalism, but for technical (not fundamental) reasons, spin-polarization is not included. This error causes an electron-pair bond to become in the order of a few kilocalories per mole too strong. To facilitate a straightforward comparison, the results of the energy decomposition were scaled to match exactly the regular bond energies. Because the Kohn−Sham MO method of DFT in principle yields exact energies and, in practice, with the available density functionals for exchange and correlation, rather accurate energies, we have the special situation that a seemingly one-particle model (a MO method) in principle completely accounts for the bonding energy.[13a]

The orbital interaction energy can be decomposed into the contributions from each irreducible representation Γ of the interacting system (eq 3) by using the extended transition state scheme developed by Ziegler and Rauk[13c−e] (note that our approach differs in this respect from the Morokuma scheme,[14]

SCHEME 1: Construction and Distortion of 1, 2, 3, and 4 in Terms of Two Rigid Fragments[a]

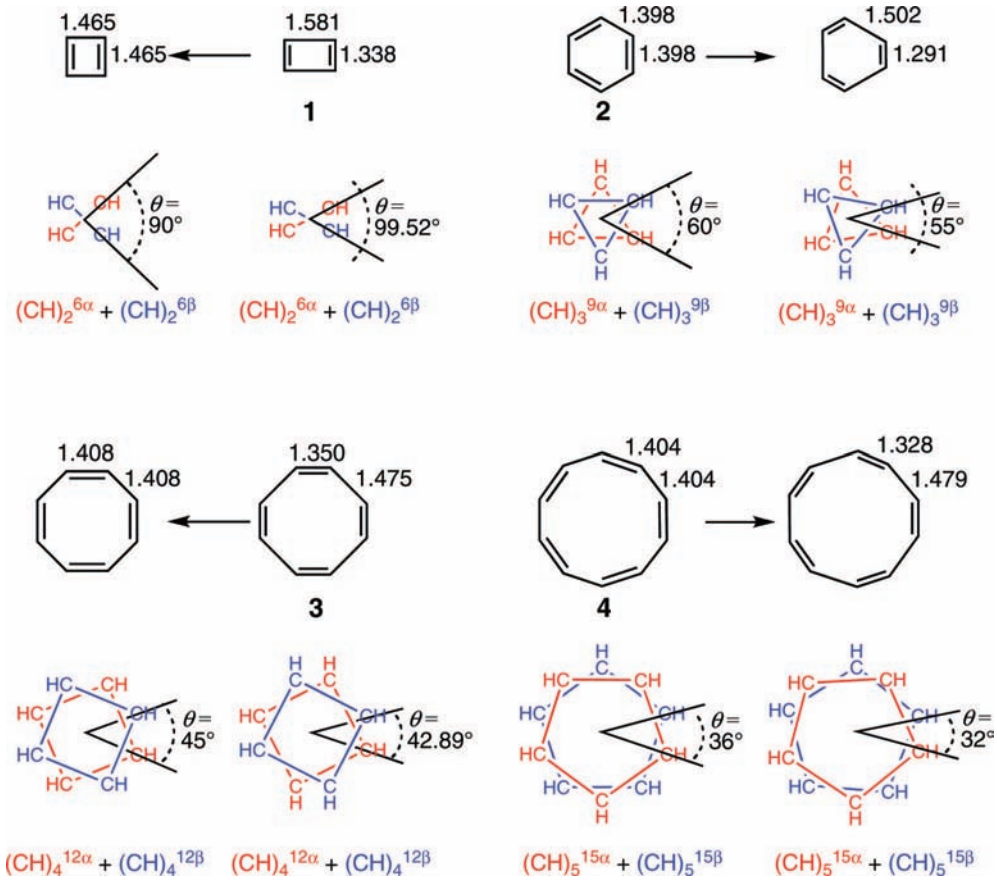

[a] Subgraphs **1** and **2** reproduced with permission from ref 3.

which instead attempts a decomposition of the orbital interactions into polarization and charge transfer).

$$\Delta E_{\mathrm{oi}} = \sum_{\Gamma} \Delta E_{\Gamma} = \Delta E_{\sigma} + \Delta E_{\pi} \qquad (3)$$

In our model systems **1**, **2**, **3**, and **4**, the irreducible representations can be categorized into symmetric and antisymmetric with respect to the mirror plane provided by the carbon-atom framework, which corresponds to what is commonly designated σ- and π-electron systems, respectively. This gives rise to the orbital-interaction components ΔE_{σ} and ΔE_{π}, as shown in eq 3 above.

3. Results and Discussions

We find that 1,3-cyclobutadiene (**1**) and benzene (**2**) have planar D_{2h} and D_{6h} symmetric equilibrium geometries: **1** has alternating short and long bonds of 1.338 and 1.581 Å, whereas **2** has six equivalent C−C bonds of 1.398 Å (see Scheme 1, upper panel). On the contrary, 1,3,5,7-cyclooctatetraene (**3′**) and 1,3,5,7,9-cyclodecapentaene (**4′**) adopt nonplanar equilibrium structures, in line with previous theoretical and experimental studies (see Introduction). We find that **3′** has the well-known tub-shaped conformation of S_4 symmetry with alternating short and long bonds of 1.345 and 1.472 Å. Likewise, **4′** adopts the saddle-shaped conformation with 10 essentially but not exactly equivalent C−C bonds of 1.40 Å. More precisely, the bond-length pattern is twice the following chain: four consecutive C−C bonds of 1.402 Å followed by one C−C bond of 1.403 Å (for complete structural information, see Table S1 in the Supporting Information). Although this differs from the pronounced bond-length alternation found by Schaefer at MP2,[11b] this result correctly indicates that **4′** still shows some aromatic character, but the latter is much reduced as compared to benzene.

Making **3′** and **4′** planar, that is, going to the corresponding planar optimum geometries **3** and **4**, is associated with a destabilization of +9.67 and +3.38 kcal/mol, respectively. However, the characteristic antiaromatic and aromatic bond-length patterns are preserved after this planarization: the planar **3** is of D_{4h} symmetry and still has alternating short and long bonds of 1.350 and 1.475 Å, whereas the planar **4** adopts D_{10h} symmetry and therefore has 10 exactly equivalent C−C bonds of 1.404 Å. The species **3** and **4** are first- and second-order saddle points, respectively. They connect two equivalent equilibrium structures **3′** and four equivalent equilibrium structures **4′**, respectively. Note also that C−C bonds in the planar **3** and **4** are always somewhat longer than the corresponding C−C bonds in the nonplanar **3′** and **4′**. We come back to this later on in the discussion.

In the following, we analyze and compare the structures and bonding of **1**, **2**, **3**, and **4**. The fact that all these species are planar enables us to consistently separate and study the bonding in the σ- and π-electron systems and how they change along the series of 4-, 6-, 8-, and 10-membered conjugated hydrocarbon rings. Later on, we will address the question why cyclooctatetraene and cyclodecapentaene eventually undergo bending and adopt nonplanar equilibrium geometries.

To understand why **1** and **3** undergo localization whereas **2** and **4** oppose localization, we have examined the energy and bonding of these species along a distortion mode proceeding from a regular delocalized structure with all C−C bonds equivalent toward a geometry with alternating single and double

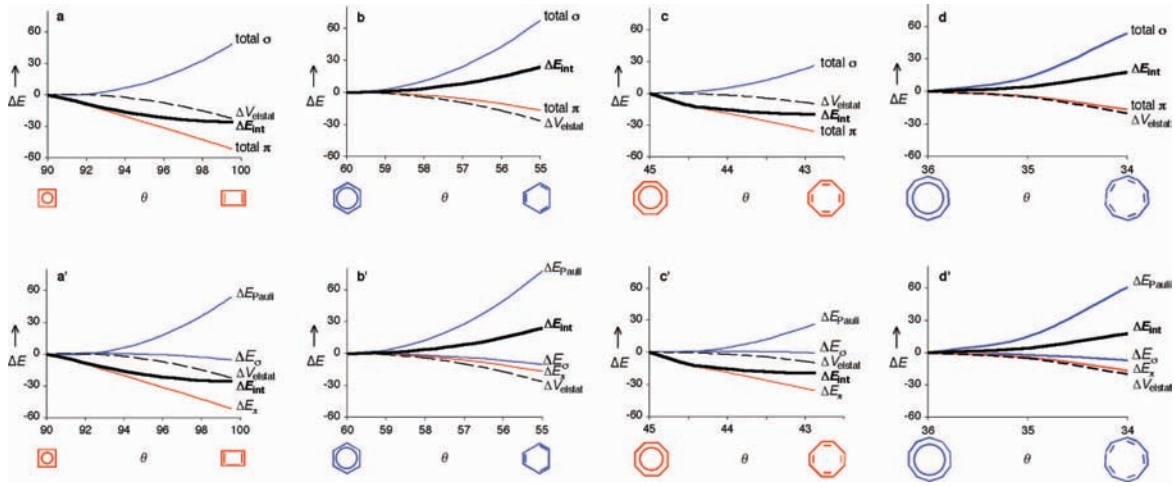

Figure 1. Bond energy decomposition (in kcal/mol) of **1**, **2**, **3**, and **4**, each constructed from two equivalent rigid fragments, as a function of the distortion mode (in degree) from delocalized to localized structure as defined in Scheme 1. $\Delta E_{int} = (\Delta E_{Pauli} + \Delta E_\sigma) + \Delta E_\pi + \Delta V_{elstat} =$ (total σ) + (total π) + ΔV_{elstat}, computed at BP86/TZ2P (subgraphs a, a′, b, and b′ reproduced with permission from ref 3).

bonds. A key step in our approach is that this can be done by rotating two equivalent and geometrically frozen fragments relative to each other, as shown in Scheme 1. Such an approach was already presented for **1** and **2** in ref 3 and is extended here to **3** and **4**. The advantage is that this greatly reduces the complexity of the bond analysis because we go from a multifragment to a two-fragment problem. Thus, for cyclobutadiene, we go from a D_{4h} symmetric species with all C−C bonds at 1.465 Å to the D_{2h} symmetric **1** with alternating C−C bonds of 1.338 and 1.581 Å. In the case of benzene, we go from D_{6h} symmetric **1** with all C−C bonds at 1.398 Å to a D_{3h} symmetric structure with alternating C−C bonds of 1.291 and 1.502 Å. Likewise, for cyclooctatetraene, we go from a D_{8h} symmetric species with all C−C bonds at 1.408 Å to the D_{4h} symmetric **3** with alternating C−C bonds of 1.350 and 1.475 Å (i.e., the optimum geometry under the constraint of planarity). And, finally, in the case of cyclodecapentaene, we go from D_{10h} symmetric **4** with all C−C bonds at 1.404 Å (which is the optimum geometry under the constraint of planarity) to a D_{5h} symmetric structure with alternating C−C bonds of 1.328 and 1.479 Å. Note that along this distortion of cyclobutadiene and cyclooctatetraene, we preserve the singlet electron configuration of the equilibrium structures **1** and **3**, because we wish to understand the behavior of the latter (the D_{4h} and D_{8h} arrangements for **1** and **3** have triplet ground states at 5.19 and 2.33 kcal/mol above **1** and **3**, respectively, with C−C bonds of 1.444 and 1.408 Å). We wish to point out that, although physically quite plausible, our choice of deformation modes, in particular the nonequilibrium localized benzene and cyclodecapentaene as well as the delocalized cyclobutadiene and cyclooctatetraene geometries, is not unique. However, we have already previously verified for cyclobutadiene and benzene that all trends and conclusions that play a role in the following discussion are not affected if other plausible choices are made.[3]

In our approach, the change in energy ΔE that goes with localizing our model systems is equal to the change in interaction energy ΔE_{int} between two geometrically frozen $(CH)_2^{6\bullet}$, $(CH)_3^{9\bullet}$, $(CH)_4^{12\bullet}$, and $(CH)_5^{15\bullet}$ fragments in their septet, decet, tredecet, and sexdecet valence configuration for **1**, **2**, **3**, and **4**, respectively. The preparation energy ΔE_{prep} vanishes in this analysis because it is constant for geometrically frozen fragments. Each pair of fragments has mutually opposite spins (superscripts α and β in Scheme 1) to allow for the formation of all σ- and π-electron pair bonds. These fragments are weakly (compared to the bonding interactions in **1**, **2**, **3**, and **4**) repulsive conglomerates of two, three, four, and five $CH^{\bullet\bullet\bullet}$ radicals, respectively. The changes in interaction can be analyzed within the conceptual framework of the MO model contained in Kohn−Sham DFT by decomposing ΔE_{int} into classical electrostatic attraction (ΔV_{elstat}), Pauli repulsive orbital interactions between same-spin electrons (ΔE_{Pauli}), and the (mainly electron-pair) bonding orbital interactions (ΔE_{oi}).[13] As pointed out in the Theoretical Methods section, the latter can be symmetry decomposed into contributions from the σ- and π-orbital interactions: $\Delta E_{oi} = \Delta E_\sigma + \Delta E_\pi$.[13] Thus, we have

$$\Delta E_{int} = \Delta E_{Pauli} + \Delta E_\sigma + \Delta E_\pi + \Delta V_{elstat} \quad (4)$$

And because in our construction of **1**, **2**, **3**, and **4**, the π electrons contribute no Pauli repulsion (vide infra), we can write

$$\Delta E_{int} = (\text{total } \sigma) + (\text{total } \pi) + \Delta V_{elstat} \quad (5)$$

with (total σ) = $\Delta E_{Pauli} + \Delta E_\sigma$ and (total π) = ΔE_π.

The results of our analyses, in Figure 1, show that not only in **1** and **2** (as shown previously)[3] but also in **3** and **4**, it is the π electrons that determine whether an aromatic, delocalized geometry or an antiaromatic geometry with localized double bonds occurs. In the first place, not unexpectedly, localization of the delocalized D_{4h} and D_{8h} symmetric arrangements of cyclobutadiene and cyclooctatetraene toward the corresponding D_{2h} and D_{4h} symmetric structures **1** and **3** goes with a stabilization, whereas the energy of D_{6h} and D_{10h} symmetric benzene (**2**) and cyclodecapentaene (**4**) rises on localization (black bold curves in Figure 1a−d). Now, it appears that the σ-electron system always opposes this localization, whereas the π-electron system always promotes the very same localization of double bonds (compare blue-(total σ) with red-(total π) curves in Figure 1a−d).

There is a marked difference between the localizing force that the respective π-electron systems exert on the ring geometry in **1** and **3** and that in **2** and **4**. In the antiaromatic ring systems **1** and **3**, the propensity of the π system to localize the double bonds is dramatically increased as compared to the aromatic rings **2** and **4** (compare red-(total π) curve in Figure 1a,c with those in Figure 1b,d). The classical electrostatic attraction ΔV_{elstat}, which slightly favors localization, differs much less along **1**−**4**.

How can we understand the result described above? The σ bonds are characterized by an equilibrium distance greater than

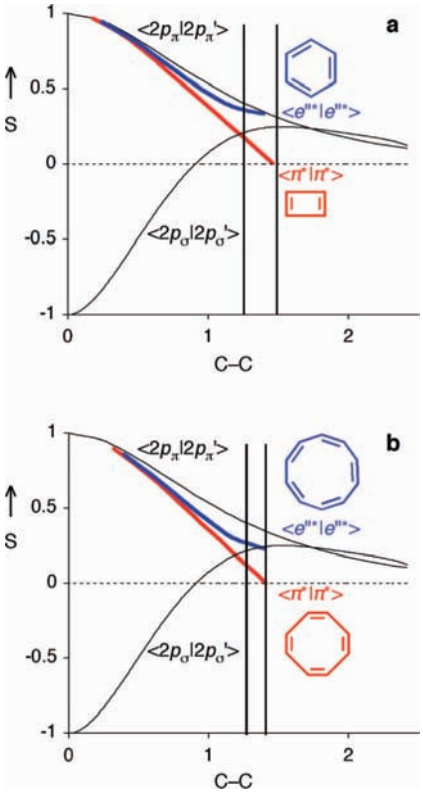

Figure 2. Selected overlap integrals between MOs of two CH$^{\bullet\bullet\bullet}$ units in **2** (black curves in a and b), between MOs of two $(CH)_2^{6\bullet}$ units in **1** (red curve in a), between two $(CH)_3^{9\bullet}$ units in **2** (blue curve in a), between MOs of two $(CH)_4^{12\bullet}$ units in **3** (red curve in b), and between two $(CH)_5^{15\bullet}$ units in **4** (blue curve in b) as a function of the C−C distance (in angstrom) along the localization distortion defined in Scheme 1. The localization interval for **1**, **2**, **3**, and **4** is indicated by vertical lines (subgraph a reproduced with permission from ref 3).

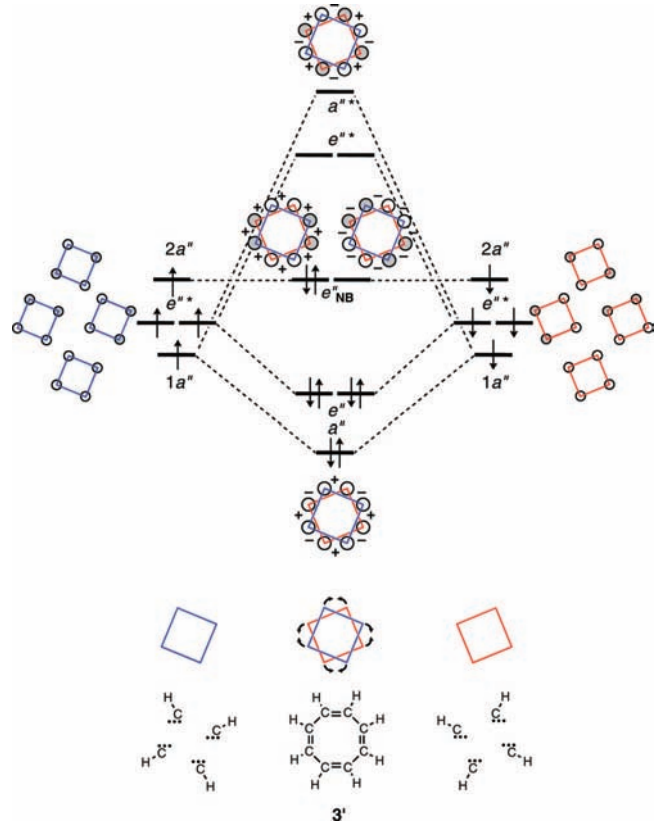

Figure 3. Schematic π MO interaction diagram of cyclooctatetraene (**3'**) constructed from two $(CH)_4^{12\bullet}$ fragments in their tredecet valence configuration, based on Kohn−Sham MO analyses at BP86/TZ2P. There are four π electrons in each of the two fragments, which have mutually opposite spin. The effect on orbital energies of the localization mode defined in Scheme 1 and represented here with curved arrows is indicated by + (stabilization) and − (destabilization).

zero, roughly 1.5 Å for C−C bonds. One reason for this is the early onset of $<2p_\sigma|2p_\sigma'>$ compared to $<2p_\pi|2p_\pi'>$ overlap and the fact that the former achieves an optimum at distances greater than zero whereas the latter is maximal at distance zero (see also ref 15). This is illustrated in Figure 2 for two C−H$^{\bullet\bullet\bullet}$ fragments in benzene approaching each other on localization (see black curves). However, as pointed out before in a different context,[16] the main reason for σ bonds to feature an optimum distance greater than zero is the repulsive wall provided by Pauli repulsion with the closed shell 2s (and 1s) atomic orbitals on carbon and the C−H bonds. In the symmetric, delocalized structures, each C−C bond is already forced by partial π bonding below the optimum σ distance; that is, it is already in the region where the Pauli repulsion ΔE_{Pauli} due to the σ electrons goes up in energy faster than the stabilizing orbital interactions ΔE_σ and ΔV_{elstat} together go down. This becomes clear if one separates (total σ), shown in Figure 1a−d, into its component $\Delta E_{\text{Pauli}} + \Delta E_\sigma$, as has been done in Figures 1a′−d′.

The π-electron systems, on the other hand, only provide electron-pair bonding and no Pauli repulsive orbital interactions, as can be seen for **3** and **4** in Figures 3 and 4 (for **1** and **2**, see Figures 5 and 4, respectively, in ref 3). They achieve an optimum overlap at zero bond distance (see Figure 2). But why is the localizing propensity of the π system in **1** and **3** so prominent whereas it is so little pronounced in **2** and **4**? Essential for understanding this difference is the qualitatively different topology and geometry dependence of the π overlaps in the aromatic or antiaromatic many-π-electron systems as compared to that of a simple two-π-electron system which is represented by the black $<2p_\pi|2p_\pi'>$ curve in Figure 2. Scheme 2 shows the key features from Figures 3 and 4 (and Figures 5 and 4 of ref 3) that emerge from our quantitative Kohn−Sham MO analyses.

The main difference between π overlap in **1**−**4** versus that between two simple CH$^{\bullet\bullet\bullet}$ fragments is the occurrence of amplifying effects, on localization, in the antiaromatic **1** and **3** and counteracting effects in the aromatic **2** and **4**. Whereas the $<2p_\pi|2p_\pi'>$ overlap between two CH$^{\bullet\bullet\bullet}$ fragments smoothly increases from 0 (at C−C = ∞) toward the value 1 (at C−C = 0), the π-bonding a″ MOs in **1**, **2**, **3**, and **4** gain and lose bonding overlap in the shrinking and expanding C−C bonds, respectively (see Scheme 2; see also Figures 3 and 4 as well as Figures 5 and 4 of ref 3). The net effect is still a gain in bonding, but in essence, this is not so pronounced anymore (see Figure 2). Similar arguments hold for the π-bonding set of degenerate e″ MOs in **2** and **4**. This is shown in Scheme 2, in which stabilizing and destabilizing effects are indicated for one of these e″ MOs with + and − signs, respectively (see Figures 3 and 4 for more details of the bonding). This makes the π systems of the aromatic ring systems **2** and **4** comparatively indifferent with respect to localizing the double C−C bonds.

A completely different situation holds for the nonbonding degenerate e''_{NB} MOs in the second-order Jahn−Teller unstable D_{4h}- and D_{8h}-symmetric geometries of cyclobutadiene and cyclooctatetraene.[15] One of these π MOs in either of the antiaromatic rings gains, on localization, stabilization in every C−C bond (this is indicated with the + signs in Scheme 2). And it does so rapidly. This is because the orbital overlap starts

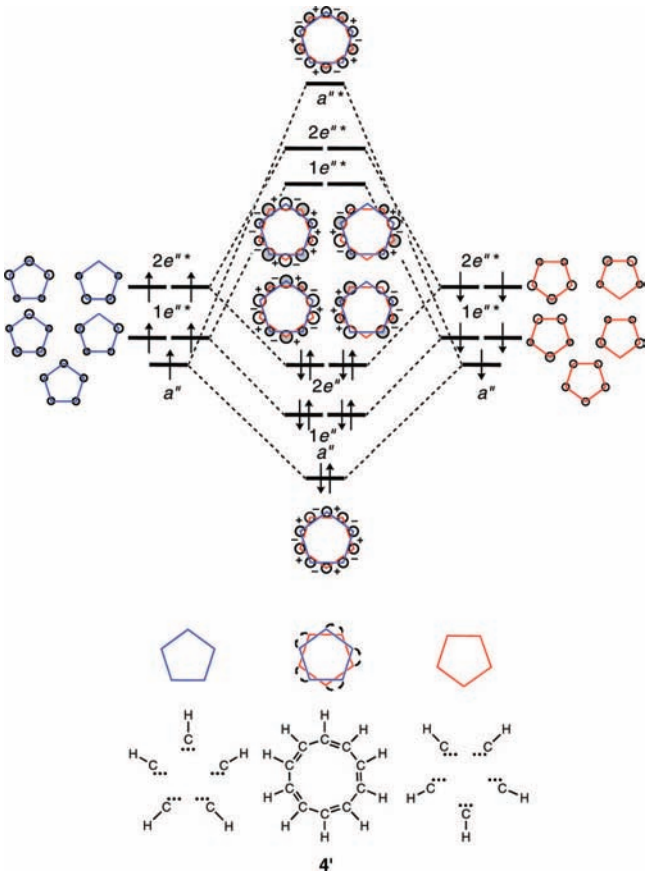

Figure 4. Schematic π MO interaction diagram of cyclodecapentaene (**4**) constructed from two $(CH)_5^{15\bullet}$ fragments in their sexdecet valence configuration, based on Kohn−Sham MO analyses at BP86/TZ2P. There are five π electrons in each of the two fragments, which have mutually opposite spin. The effect on orbital energies of the localization mode defined in Scheme 1 and represented here with curved arrows is indicated by + (stabilization) and − (destabilization).

to build up from 0 (i.e., no overlap and no stabilization) at a finite C−C distance of 1.465 Å (**1**) or 1.408 Å (**3**) and rises to the value 1 as the C−C distance decreases to 0 (see Figure 2). This differs from the distance dependence of the π overlap between two $2p_\pi$ AOs on two simple $CH^{\bullet\bullet\bullet}$ fragments (or on two carbon atoms) which has its zero point at a C−C distance of ∞ but also goes to 1 as the C−C distance decreases to 0 Å (see $<2p_\pi|2p_\pi'>$ in Figure 2). Along the bond localizing distortion, the gain in overlap in **1** between the two π^* $(CH)_2^{6\bullet}$ fragment MOs (see Figure 5 in ref 3) is a sizeable 0.102! (see Figure 2a). Likewise, although somewhat less pronounced, the gain in overlap in **3** between the two π^* $(CH)_4^{12\bullet}$ fragment MOs amounts to 0.051 (see Figure 2b). This has to be compared with a much smaller gain in overlap of only 0.012 and 0.020 between the two e''^* $(CH)_3^{9\bullet}$ fragment MOs in **2** and the two e'' $(CH)_5^{15\bullet}$ fragment MOs in **4**, respectively, that form the π bonding e″ HOMOs of the two aromatic rings. Consequently, the aforementioned e''_{NB} MO of cyclobutadiene and that of cyclooctatetraene, which are fully occupied in the singlet ground state of **1** and **3**, drop markedly in energy along the localization mode. This causes the enhanced propensity of the π-electron system in cyclobutadiene and cyclooctatetraene toward localization of the double C−C bonds.

Finally, we come back to the question why cyclooctatetraene and cyclodecapentaene eventually undergo bending and adopt nonplanar equilibrium geometries **3′** and **4′**. This phenomenon can be ascribed to the increased steric repulsion between

SCHEME 2: Effect of Localization on π MO Levels of 1, 2, 3, and 4[a]

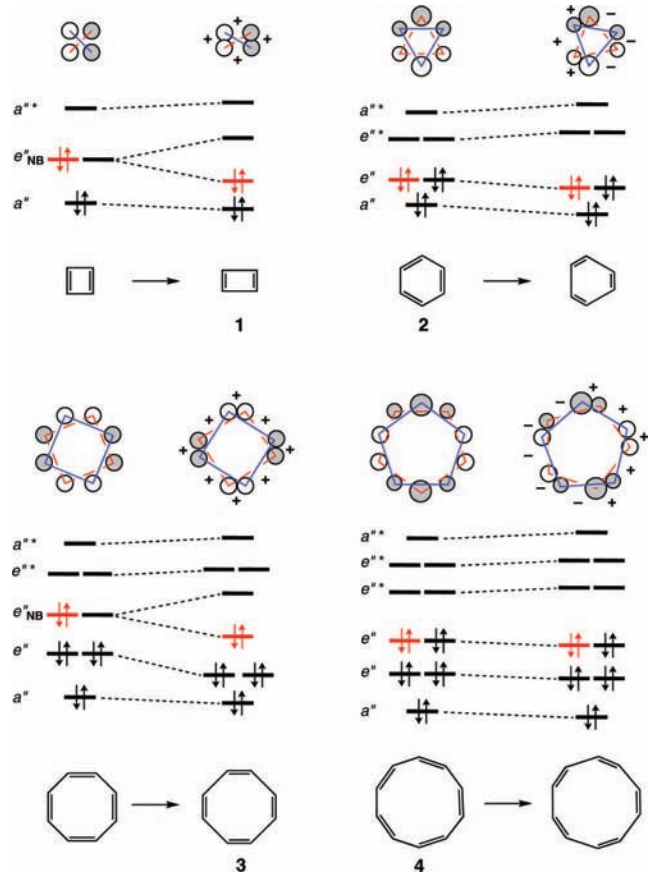

[a] Orbital plots at top refer to red levels (subgraphs **1** and **2** reproduced with permission from ref 3).

hydrogens of vicinal C−H bonds, very similar to the mechanism that causes ethane to avoid the eclipsed C−H bonds and to adopt a staggered conformation.[16a,c] Thus, along the series **1**, **2**, **3**, and **4**, the longest vicinal H−H distance in each of these planar species decreases monotonically from 3.115 to 2.488 to 2.271 to 2.080 Å because the C−C−H angle systematically decreases, for simple goniometric reasons, as the size of the carbon ring becomes larger.[17] The increasing H−H steric repulsion can be relieved in **3** through facile internal rotation of C−H bonds around C−C single bonds (H−C−C−H = 42.6°) but not around the localized C−C double bonds (H−C−C−H = 0°), yielding the tub-shaped **3′**. Likewise, the further increasing H−H steric repulsion in **4** can again be reduced through internal rotation of C−H bonds around C−C bonds. But at variance with **3**, the C−C bonds all have partial double-bond character, yielding the saddle-shaped **4′** in which the bending is spread over more −CH−CH− moieties with smaller dihedral angles (two times 14.4, 12.8, −6.3, −17.1, and −3.9°). Note that the diminished H−H repulsion in the nonplanar **3′** and **4′** also translates into the slight contraction of C−C bonds (as compared to planar **3** and **4**, respectively) mentioned in the beginning of the discussion.

4. Conclusions

The MO model of (anti)aromaticity that we recently developed[3] for cyclobutadiene (**1**) and benzene (**2**) extends also to the corresponding next larger analogues, cyclooctatetraene (**3′**) and cyclodecapentaene (**4′**), respectively. Our MO model accounts for the antiaromaticity of **3′** and the only very weakly aromatic nature of **4′**.

Thus, in none of the cases does the π-electron system favor a symmetric, delocalized ring. The regular, symmetric structure of benzene has the same cause as that of cyclohexane,[3] namely, the σ-electron system. Nevertheless, the π system determines whether delocalization occurs by showing qualitatively different geometry-dependence of the π overlap in the aromatic (**2** and **4′**) versus the antiaromatic (**1** and **3′**) rings. In the latter two, all π-overlap effects unidirectionally favor localization of the double bonds and can, in this way, overrule the σ system. The somewhat more pronounced steric repulsion between vicinal C−H bonds in planar **3** causes cyclooctatetraene to adopt the nonplanar, tub-shaped equilibrium conformation **3′** in which this steric repulsion is reduced around C−C single bonds.

In the aromatic species, the localizing propensity of the π system emerges from a subtle interplay of counteracting overlap effects. In benzene (**2**), it is therefore too little pronounced to overcome the delocalizing σ system. In cyclodecapentaene, the π system shows a somewhat increased localizing propensity, but in our BP86 calculations, this is still not strong enough to overcome the delocalizing σ system. Therefore, we arrive at a delocalized structure which, however, adopts a nonplanar, saddle-shaped conformation **4′** to minimize the steric repulsion between vicinal C−H bonds. Note that although our delocalized structure of **4′** differs from the MP2 geometry (with localized double bonds) found by Schaefer,[11b] our electronic-structure analyses nicely confirm that the π-electron system of **4′** causes the aromatic character of this species to be much reduced if compared to **2**.

Acknowledgment. We thank the Netherlands Organization for Scientific Research (NWO-CW and NWO-NCF) for financial support.

Supporting Information Available: Complete structural information. This material is available free of charge via the Internet at http://pubs.acs.org.

References and Notes

(1) (a) Garratt, P. J. *Aromaticity*; John Wiley & Sons, Inc.: New York, 1986. (b) Minkin, V. I.; Glukhotsev, M. N.; Simkin, B. Y. *Aromaticity and Antiaromaticity: Electronic and Structural Aspects*; John Wiley & Sons, Inc.: New York, 1994.

(2) (a) Breslow, R. *Acc. Chem. Res.* **1973**, *6*, 393. (b) Bickelhaupt, F.; de Wolf, W. H. *Recl. Trav. Chim. Pays-Bas* **1988**, *107*, 459. (c) Kraakman, P. A.; Valk, J.-M.; Niederländer, H. A. G.; Brouwer, D. B. E.; Bickelhaupt, F. M.; de Wolf, W. H.; Bickelhaupt, F.; Stam, C. H. *J. Am. Chem. Soc.* **1990**, *112*, 6638. (d) Krygowski, T. M.; Cyranski, M. K.; Czarnocki, Z.; Hafelinger, G.; Katritzky, A. R. *Tetrahedron* **2000**, *56*, 1783. (e) Schleyer, P. v. R.; Jiao, H. J. *Pure Appl. Chem.* **1996**, *68*, 209. (f) Special issue on Aromaticity. Schleyer, P. v. R., Ed. , *Chem. Rev.* **2001**, *101*. (g) Cyranski, M. K.; Krygowski, T. M.; Katritzky, A. R.; Schleyer, P. v. R. *J. Org. Chem.* **2002**, *67*, 1333. (h) Special issue on Delocalization−Pi and Sigma. Gladysz, J. A., Ed. , *Chem. Rev.* **2005**, 105. (i) Moran, D.; Simmonett, A. C.; Leach, F. E., III.; Allen, W. D.; Schleyer, P. v. R.; Schaefer, H. F., III *J. Am. Chem. Soc.* **2006**, *128*, 9342.

(3) Pierrefixe, S. C. A. H.; Bickelhaupt, F. M. *Chem. Eur. J.* **2007**, *13*, 6321.

(4) Hückel, E. *Z. Phys.* **1931**, *70*, 204.

(5) (a) Smith. M. B., March J. *March's Advanced Organic Chemistry*, 6th ed.; Wiley-Interscience: New York, 2007. (b) Carey, F. A.; Sundberg, R. J. *Advanced Organic Chemistry: Structure And Mechanisms (Part A)*; Springer: New York, 2000.

(6) (a) Ooshika, Y. *J. Phys. Soc. Jpn.* **1957**, *12*, 1238. (b) Labhart, H. *J. Chem. Phys.* **1957**, *27*, 947. (c) Longuet-Higgins, H. C.; Salem, L. *Proc. R. Soc. London, Ser. A* **1959**, *251*, 172. (d) Tsui, M.; Huzinaga, S.; Hasino, T. *Rev. Mod. Phys.* **1960**, *32*, 425. (e) Berry, R. S. *J. Chem. Phys.* **1961**, *35*, 2253.

(7) (a) Haas, Y.; Zilberg, S. *J. Am. Chem. Soc.* **1995**, *117*, 5387. (b) Heilbronner, E. *J. Chem. Educ.* **1989**, *66*, 471. (c) Stanger, A.; Vollhardt, K. P. C. *J. Org. Chem.* **1988**, *53*, 4889. (d) Epiotis, N. D. *Pure Appl. Chem.* **1983**, *55*, 229.

(8) (a) Hiberty, P. C.; Shaik, S. S.; Lefour, J. M.; Ohanessian, G. *J. Org. Chem.* **1985**, *50*, 4657. (b) Shaik, S. S.; Hiberty, P. C. *J. Am. Chem. Soc.* **1985**, *107*, 3089. (c) Hiberty, P. C.; Shaik, S. S.; Ohanessian, G.; Lefour, J. M. *J. Org. Chem.* **1986**, *51*, 3908. (d) Shaik, S. S.; Hiberty, P. C.; Lefour, J. M.; Ohanessian, G. *J. Am. Chem. Soc.* **1987**, *109*, 363. (e) Shaik, S. S.; Hiberty, P. C.; Ohanessian, G.; Lefour, J. M. *J. Phys. Chem.* **1988**, *92*, 5086. (f) Hiberty, P. C.; Danovich, D.; Shurki, A.; Shaik, S. *J. Am. Chem. Soc.* **1995**, *117*, 7760. (g) Shurki, A.; Shaik, S. *Angew. Chem., Int. Ed. Engl.* **1997**, *36*, 2205. (h) Shaik, S.; Shurki, A.; Danovich, D.; Hiberty, P. C. *Chem. Rev.* **2001**, *101*, 1501.

(9) (a) Baird, N. C. *J. Org. Chem.* **1986**, *51*, 3907. (b) Glendening, E. D.; Faust, R.; Streitwieser, A.; Vollhardt, K. P. C.; Weinhold, F. *J. Am. Chem. Soc.* **1993**, *115*, 10952.

(10) (a) Jug, K.; Koster, A. M. *J. Am. Chem. Soc.* **1990**, *112*, 6772. (b) Gobbi, A.; Yamaguchi, Y.; Frenking, G.; Schaefer, H. F., III *Chem. Phys. Lett.* **1995**, *244*, 27. (c) Kovačević, B.; Barić, D.; Maksić, Z. B.; Müller, T. *ChemPhysChem* **2004**, *5*, 1352. (d) Rehaman, A.; Datta, A.; Mallajosyula, S. S.; Pati, S. K. *J. Chem. Theory Comput.* **2006**, *2*, 30.

(11) (a) Karadakov, P. B.; Gerratt, J.; Cooper, D. L.; Raimondi, M. *J. Phys. Chem.* **1995**, *99*, 10186. (b) King, R. A.; Crawford, T. D.; Stanton, J. F.; Schaefer, H. F., III *J. Am. Chem. Soc.* **1999**, *121*, 10788.

(12) (a) te Velde, G.; Bickelhaupt, F. M.; Baerends, E. J.; Fonseca Guerra, C.; van Gisbergen, S. J. A.; Snijders, J. G.; Ziegler, T. *J. Comput. Chem.* **2001**, *22*, 931. (b) Fonseca Guerra, C.; Visser, O.; Snijders, J. G.; te Velde, G.; Baerends, E. J. In *Methods and Techniques for Computational Chemistry*, Clementi, E., Corongiu, G., Eds.; STEF: Cagliari, 1995, pp 305–395. (c) Baerends, E. J.; Ellis, D. E.; Ros, P. *Chem. Phys.* **1973**, *2*, 41. (d) Baerends, E. J.; Ros, P. *Chem. Phys.* **1975**, *8*, 412. (e) Baerends, E. J.; Ros, P. *Int. J. Quantum Chem. Symp.* **1978**, *12*, 169. (f) Fonseca Guerra, C.; Snijders, J. G.; te Velde, G.; Baerends, E. J. *Theor. Chem. Acc.* **1998**, *99*, 391. (g) Boerrigter, P. M.; te Velde, G.; Baerends, E. J. *Int. J. Quantum Chem.* **1988**, *33*, 87. (h) te Velde, G.; Baerends, E. J. *J. Comput. Phys.* **1992**, *99*, 84. (i) Snijders, J. G.; Baerends, E. J.; Vernooijs, P. *At. Nucl. Data Tables* **1982**, *26*, 483. (j) Krijn, J.; Baerends, E. J. *Fit-Functions in the HFS-Method; Internal Report* (in Dutch); Vrije Universiteit: Amsterdam, 1984. (k) Versluis, L.; Ziegler, T. *J. Chem. Phys.* **1988**, *88*, 322. (l) Slater, J. C. *Quantum Theory of Molecules and Solids*; McGraw-Hill: New York, 1974; *Vol. 4*. (m) Becke, A. D. *J. Chem. Phys.* **1986**, *84*, 4524. (n) Becke, A. *Phys. Rev. A* **1988**, *38*, 3098. (o) Vosko, S. H.; Wilk, L.; Nusair, M. *Can. J. Phys.* **1980**, *58*, 1200. (p) Perdew, J. P. *Phys. Rev. B* **1986**, *33*, 8822 Erratum: *Phys. Rev. B* **1986**, *34*, 7406). (q) Fan, L.; Ziegler, T. *J. Chem. Phys.* **1991**, *94*, 6057.

(13) (a) Bickelhaupt, F. M.; Baerends, E. J. In *Reviews in Computational Chemistry*; Lipkowitz, K. B., Boyd, D. B., Eds.; Wiley-VCH: New York, **2000**; Vol. 15, pp 1–86. (b) Bickelhaupt, F. M.; Nibbering, N. M. M.; van Wezenbeek, E. M.; Baerends, E. J. *J. Phys. Chem.* **1992**, *96*, 4864. (c) Bickelhaupt, F. M.; Diefenbach, A.; de Visser, S. P.; de Koning, L. J.; Nibbering, N. M. M. *J. Phys. Chem. A* **1998**, *102*, 9549. (d) Ziegler, T.; Rauk, A. *Inorg. Chem.* **1979**, *18*, 1755. (e) Ziegler, T.; Rauk, A. *Inorg. Chem.* **1979**, *18*, 1558. (f) Ziegler, T.; Rauk, A. *Theor. Chim. Acta* **1977**, *46*, 1.

(14) Morokuma, K. *Acc. Chem. Res.* **1977**, *10*, 294.

(15) Albright, T. A.; Burdett, J. K.; Whangbo, M.-H. *Orbital Interactions in Chemistry*; John Wiley & Sons Inc: New York, 1985.

(16) (a) Bickelhaupt, F. M.; Baerends, E. J. *Angew. Chem.* **2003**, *115*, 4315. Bickelhaupt, F. M.; Baerends, E. J. *Angew. Chem. Int. Ed.* **2003**, *42*, 4183. (b) Bickelhaupt, F. M.; DeKock, R. L.; Baerends, E. J. *J. Am. Chem. Soc.* **2002**, *124*, 1500. (c) Mo, Y.; Gai, J. *Acc. Chem. Res.* **2007**, *40*, 113.

(17) This C−C−H angle is 150° for D_{3h} symmetric C_3H_3 and approaches the limiting value of 90° if $n \rightarrow \infty$ for D_{nh} symmetric C_nH_n.

JP800514N